HMG Advance Access published August 17, 2010

Oxidative stress by monoamine oxidases is causally involved in myofiber damage in muscular dystrophy

Sara Menazza[1], Bert Blaauw[2,3], Tania Tiepolo[4], Luana Toniolo[3], Paola Braghetta[4], Barbara Spolaore[5], Carlo Reggiani[3], Fabio Di Lisa[1], Paolo Bonaldo[4] & Marcella Canton[1*]

[1]Department of Biomedical Sciences, University of Padova, 35131 Padova, Italy, [2]Venetian Institute of Molecular Medicine, 35129 Padova, Italy, Departments of [3]Human Anatomy & Physiology and of [4]Histology, Microbiology & Medical Biotechnologies, University of Padova, 35131 Padova, Italy, [5]CRIBI Biotechnology Centre, 35131 Padova, Italy .

* To whom correspondence should be addressed. Tel +39 049 8276084; Fax +39 049 8276079; Email bonaldo@bio.unipd.it (P. B.); Tel +39 049 8276414; Fax +39 049 8276040; E-mail marcella.canton@unipd.it (M.C.)

Abstract

Several studies documented the key role of oxidative stress and abnormal production of reactive oxygen species (ROS) in the pathophysiology of muscular dystrophies (MDs). The sources of ROS, however, are still controversial as well as their major molecular targets. This study investigated whether ROS produced in mitochondria by monoamine oxidase (MAO) contributes to MD pathogenesis. Pargyline, a MAO inhibitor, reduced ROS accumulation along with a beneficial effect on the dystrophic phenotype of *Col6a1*$^{-/-}$ mice, a model of Bethlem myopathy and Ullrich congenital MD, and *mdx* mice, a model of Duchenne MD. Based on our previous observations on oxidative damage of myofibrillar proteins in heart failure, we hypothesized that MAO-dependent ROS might impair contractile function in dystrophic muscles. Indeed, oxidation of myofibrillar proteins, as probed by formation of disulphide cross-bridges in tropomyosin, was detected in both *Col6a1*$^{-/-}$ and *mdx* muscles. Notably, pargyline significantly reduced myofiber apoptosis and ameliorated muscle strength in *Col6a1*$^{-/-}$ mice. This study demonstrates a novel and determinant role of MAO in MDs, adding evidence of the pivotal role of mitochondria and suggesting a therapeutic potential for MAO inhibition.

Introduction

Muscle dystrophies (MDs) are a heterogeneous group of inherited human disorders primarily affecting skeletal muscles. Typically, MDs show diffuse wasting and weakness of muscles, associated with degeneration and regeneration of muscle fibers. Duchenne muscular dystrophy is the most common and severe form of MD worldwide. This progressive and lethal X-linked myopathy is characterized by deficiency of dystrophin, a subsarcolemmal protein critical in membrane stabilization and prevention of contraction-induced cell membrane damage (1).

Although mutations in components of the dystrophin glycoprotein complex are responsible for the most devastating MDs, mutations of genes coding for extracellular matrix proteins play a causative role in other forms of MDs. Indeed, another group of MDs is due to inherited mutations in genes encoding collagen VI. Collagen VI is a major component of the endomysium, where it is localized just outside the basement membrane of muscle fibers. Mutations of Collagen VI cause two muscle diseases in humans, namely Bethlem myopathy (MIM#158810) and Ullrich congenital muscular dystrophy (MIM#254090) (2). Bethlem myopathy is a relatively mild and slowly progressive myopathic disorder, whereas UCMD is a severe and rapidly progressive muscle disease usually causing early death due to respiratory failure.

Several studies documented the key role of oxidative stress and abnormal production of ROS in the pathophysiology of MDs (3-6). Antioxidant treatments have been shown to counteract myocyte injury in *mdx* mice demonstrating the key role of reactive oxygen species (ROS) in MD pathogenesis (7). Indeed, ROS formation appears a causative event rather than a consequence of muscle degeneration (8). Mitochondria are generally indicated as a major source of ROS. In fact, recent studies provided clear evidence of the crucial role of mitochondria in MDs. This concept is supported by genetic or pharmacological reduction of the open probability of the mitochondrial permeability transition pore,

that has been demonstrated to prevent myofiber injury characterizing experimental models of MDs (9-11).

Besides the respiratory chain, a relevant source of ROS in mitochondria is represented by monoamine oxidases (MAO). These flavoproteins, which exist in two isoforms, MAO-A and MAO-B, are located in the outer mitochondrial membrane and catalyze the oxidative deamination of neurotransmitters and dietary amines, generating hydrogen peroxide (12). The monoamine catabolism generates aldehydes, ammonia and hydrogen peroxide. MAO has been extensively studied at the level of the central nervous system while their role in other tissues has been scarcely investigated. Nevertheless, evidence has been provided that MAO contributes to cardiac diseases (13,14). As far as the targets of ROS are concerned, we hypothesized the myofibrillar proteins could represent important intracellular targets of ROS involved in contractile dysfunction of the dystrophic muscle. Indeed, in several models of myocardial dysfunction, such as coronary microembolization and heart failure, we demonstrated that myofibrillar proteins, such as tropomyosin (Tm), actin and desmin were modified by ROS and that the contractile impairment was related to formation of disulphide cross-bridges in Tm (15,16).

In the present study we investigated the role of MAO in skeletal muscles of two murine models for different forms of MDs, namely *Col6a1*$^{-/-}$ and *mdx* mice. Our findings demonstrate that accumulation of ROS related to MAO activity plays a pivotal role in both loss of cell viability and contractile derangements of dystrophic skeletal muscles. This is supported by the protective efficacy of the MAO inhibitor pargyline on oxidative stress, alterations of muscle structure and function, and loss of cell viability in the two murine MD models.

Results

Myofibrillar protein oxidation in *Col6a1*$^{-/-}$ mice and effects of MAO inhibition

Two murine models of MD were considered in this study: *Col6a1*$^{-/-}$ mice, which lack collagen VI due to null mutation of the gene coding for the α1(VI) subunit (2), and *mdx* mice which lack dystrophin (17). We first investigated the activity of MAO in skeletal muscle and found that it was significantly increased in six-month-old *Col6a1*$^{-/-}$ mice as compared to wild-type littermates (Figure 1A). The increased MAO activity was associated with an increase of MAO-A protein levels in *Col6a1*$^{-/-}$ muscle (Figure 1B). To assess the role of MAO-dependent ROS accumulation, *Col6a1*$^{-/-}$ mice were randomized into groups receiving i.p. treatment with pargyline (50 mg/kg/d), a MAO-A and MAO-B inhibitor, or vehicle for one week. MAO activity was abolished after the treatment (Figure 1A).

Next, we quantified ROS production in six-month-old *Col6a1*$^{-/-}$ mice. When compared to age-matched wild-type mice, muscles of *Col6a1*$^{-/-}$ mice showed an increased accumulation of ROS, as revealed by increased dihydroethidium (DHE) fluorescence in diaphragm and gastrocnemius (Fig 1C). Importantly, the abnormal production of ROS in *Col6a1*$^{-/-}$ muscles was significantly decreased upon pargyline treatment (Figure 1C and D).

Then, we investigated whether MAO-dependent ROS accumulation caused oxidative modifications of myofibrillar proteins, as probed by Tm oxidation. Indeed, we previously demonstrated that, among myofibrillar proteins, Tm is particularly susceptible to oxidative stress (16). Immunoblots with anti-Tm displayed additional high molecular mass bands in *Col6a1*$^{-/-}$ diaphragm, which is the most affected muscle in this murine model (Figure 2A). The appearance of these bands, which were much fainter in samples obtained from wild-type littermates, reflected disulfide cross-bridges (DCB) formation because they were visible only under non-reducing electrophoresis. The band at 82 kDa was attributed to a dimer of Tm, while the bands with an apparent molecular mass > 220 kDa could reflect high

molecular mass complexes among several monomers of Tm, or between Tm and other proteins. It is worth pointing out that skeletal Tm contains the α- as well as the β-isoform. At variance from the presence of a single cysteine in the α-isoform, β-Tm contains two Cys residues that might result in the covalent aggregation of more than two proteins by means of DCB formation. Indeed mass spectrometric analysis performed on the high molecular mass Tm complexes identified the myosin heavy chain (Supplemental Table). DCB content was 3.2±0.4 fold higher in *Col6a1*$^{-/-}$ as compared to wild-type muscles and was significantly reduced by pargyline treatment (Figure 2B).

MAO inhibition ameliorates muscle apoptotic phenotype of *Col6a1*$^{-/-}$ mice

Contractile impairment and high apoptosis rate are two specific features of skeletal muscles of *Col6a1*$^{-/-}$ mice (11). We therefore investigated whether pargyline treatment was able to improve cell survival and to counteract the apoptotic phenotype observed in *Col6a1*$^{-/-}$ mice. Occurrence of apoptosis was evaluated by the terminal deoxynucleotidyl transferase-mediated dUTP nick end labeling (TUNEL). The number of TUNEL-positive nuclei was higher in *Col6a1*$^{-/-}$ mice as compared to wild-type littermates (62.4±2.3 versus 2.7±1.2 nuclei/mm^2), and pargyline treatment reduced the occurrence of TUNEL-positive nuclei to a level (6.9±1) that was not significantly different from that observed in wild-type mice (Figure 3A). Direct evidence of a protective effect of MAO inhibition on muscle damage was provided by immunohistochemical staining of skeletal muscle with IgG antibody. In fact, the circulating IgG can enter into the myfibers of dystrophic mice due to altered sarcolemma integrity, thus allowing their detection by FITC-conjugated anti-mouse IgG (18,19). Damaged fibers, positive to the immunohistochemical staining for IgG, were present in *Col6a1*$^{-/-}$ diaphragm and their number was significantly decreased by pargyline treatment (Figure 3B). Additional evidence of muscle damage and protection by MAO inhibition was provided by vital staining with Evans blue. Supporting the finding obtained by permeability to IgG, several damaged myofibers stained by Evans blue were found in

Col6a1$^{-/-}$ but not in wild-type diaphragm, and this alteration was largely reduced in the diaphragm of *Col6a1*$^{-/-}$ mice treated with pargyline (Figure 3C). Morphometric analysis of myofiber cross-sectional areas in tibialis anterior and diaphragm showed that *Col6a1*$^{-/-}$ muscles contained myofibers of different sizes, with a prevalence of small fibers. This pathological sign was markedly reduced in pargyline-treated *Col6a1*$^{-/-}$ muscles, which showed more uniform fiber size, similarly to wild-type mice (Figure 3D and E).

MAO inhibition ameliorates muscle dysfunction in *Col6a1*$^{-/-}$ mice.

Biochemical and histological analyses were paralleled by functional assessment of the contractile performance of muscles *in vivo* and isolated muscle fibers *in vitro*. Single skinned muscle fibers dissected from gastrocnemius muscle were maximally calcium-activated at optimal sarcomere length. *Col6a1*$^{-/-}$ fibers developed lower isometric tension than wild-type fibers, as previously reported (11,20). The contractile impairment disappeared in the fibers of pargyline-treated *Col6a1*$^{-/-}$ mice (Figure 4A). This *in vitro* evidence was further supported by *in vivo* findings, as pargyline treatment significantly increased the normalized force of gastrocnemius muscle of *Col6a1*$^{-/-}$ mice (Figure 4B). We finally tested whether treatment with pargyline could improve the voluntary exercise performance of *Col6a1*$^{-/-}$ mice, tested by means of running-wheel. After acclimatizing mice for one week to a wheel placed in their cage, we measured the daily average distance. The pargyline-treated *Col6a1*$^{-/-}$ mice showed a significant improvement in the exercise performance compared to untreated mice (Figure 4C).

MAO inhibition rescues dystrophic phenotype in *mdx* mice

The findings obtained in *Col6a1*$^{-/-}$ mice prompted us to investigate whether ROS generated by MAO might play a role also in *mdx* mice, where ROS accumulation has been previously demonstrated (5,8) Interestingly, MAO activity increased in gastrocnemius muscle of *mdx* mice along with an increase in

MAO-A protein levels (Supplemental Figure), in accordance to what observed in *Col6a1*$^{-/-}$ mice. Gastrocnemius and quadriceps of five-week-old *mdx* mice displayed a significant increase in both ROS formation and Tm oxidation (Table 1 and Figure 5A). In fact, DCB increased by 2.84±0.31 and 2.34±0.28 folds in gastrocnemius and quadriceps muscle, respectively. Importantly, these oxidative modifications were significantly decreased after i.p. treatment with pargyline for one week (Figure 5B). Morphometric analysis of myofiber cross-sectional areas in gastrocnemius muscle confirmed that *mdx* contained myofibers of different sizes, with a significant incidence of small fibers, while pargyline normalized the fiber area distribution (Figure 6A and B). In addition, pargyline was able to reduce tissue inflammation occurring in *mdx* skeletal muscles (Figure 6A). The occurrence of apoptosis was markedly increased in *mdx* mice, yet pargyline treatment led to a significantly lower incidence in the number of TUNEL-positive nuclei of *mdx* mice (Figure 6C). Taken together, these results indicate that also in *mdx* mice ROS generated by MAO are relevant to the dystrophic mechanism and that MAO inhibition protects dystrophic skeletal muscle by reducing myofiber degeneration and ROS production.

Discussion

The present study demonstrates that MAO is a major source of ROS in two murine models of MDs and that its inhibition is able to reduce the occurrence of myofibrillar protein oxidation and myofiber defects. In addition, beside reducing biochemical and histological alterations, MAO inhibition ameliorates contractile performance highlighting the relevance of mitochondrial ROS formation in MDs. Indeed the present study lends support to the concept, developed in cardiac studies (14), that oxidative stress induced by mitochondrial dysfunction causes both loss of vitality and contractile impairment partly related to the oxidation of myofibrillar proteins.

Although the loss of muscle strength in MDs is partly due to myofiber degeneration, the loss of cell viability is not sufficient to explain entirely the impairment in contractile performance of dystrophic muscles. Additional components have to contribute, since tension development is significantly decreased not only in structurally abnormal fibers, but also in fibers without any detectable sign of degeneration, particularly in skeletal muscles of *Col6a1*$^{-/-}$ mice (11). Similar observations of force loss in apparently undamaged fibers of dystrophic muscles have been reported also in other animal models (21). These findings imply that force loss is directly related with an impaired myofibrillar mechanism of force generation. It is likely that downstream the specific primary biochemical defect (the mutation and its direct impact on the protein) several cell processes are affected within muscle fibers. Oxidative stress, minimal mechanical damage and cell death have been proposed as mechanisms causing the loss of contractile force in MDs (2,3,5-9,22,23). Besides contributing to cell death, the accumulation of ROS is likely to alter the mechanical function of myofibers by means of protein modifications.

In this respect we investigated whether myofibrillar proteins can represent intracellular targets of ROS causing the contractile impairment *Col6a1*$^{-/-}$ mice muscles. The oxidative processes affect most amminoacid residues. Cys and Met residues are particularly sensitive to oxidation by ROS and generate disulfides and sulfoxide, respectively (24). Indeed, we previously found that contractile proteins, such

as actin and Tm, undergo both reversible and irreversible oxidative processes during myocardial ischemia and reperfusion (15). Moreover, we have recently demonstrated that the extent of protein oxidation correlates with the degree of contractile impairment in pigs subjected to coronary microembolization (16). The present results show that oxidation at the level of Cys residues also occurred in dystrophic muscles. Tm oxidation was detected as high-molecular-weight bands in western blots performed under non-reducing conditions. Tm oxidation is likely to hamper contractility. This hypothesis is supported by the localization of Cys residues. In fact, Cys190 is located at the interface with troponin T and DCB formation is likely to alter protein interactions that are crucial for contractile activity. This concept is supported by experimental models and clinical findings relating Tm alterations to contractile impairment (25). Although the amount of oxidized Tm is relatively modest, it has to be pointed out that severe contractile abnormalities have been reported for cardiomyocytes harboring a minor fraction of altered myofibrillar proteins. Indeed, this was the case with the original report of inborn error of Tm (26). Actually, the determination of the contractile performance *in vivo* and *in vitro* gave support to the idea that the impairment is counteracted by pargiline treatment which reduces ROS production and accumulation.

Besides altering myofibrillar proteins, oxidative stress has been associated with an increased occurrence of cell death. While lending support to the concept that mitochondria are the most relevant cellular site for ROS formation, the protective role elicited by MAO inhibition indicates that oxidative stress is causally linked to both contractile dysfunction and cell death characterizing MDs. In addition, MAO-induced ROS formation further supports the crucial contribution of mitochondria to MDs pathophysiology suggested by recent reports (9-11). In fact, mitochondria have recently received attention due to the demonstrated role of the permeability transition pore (PTP) in MDs. PTP inhibition was found to limit histological alterations in *Col6a1*$^{-/-}$ (11) as well as *mdx* (9) mice and pilot studies have demonstrated the therapeutic efficacy of PTP inhibitors, namely cyclosporin A and Debio 025

(9,23,27-29). Furthermore, ablation of cyclophilin D, a mitochondrial protein that increases the PTP open probability, prevents biochemical and structural alterations observed in different MD models (9,10). However, at present it is still difficult to link changes occurring at the level of plasma membrane or even outside the cell, such as loss of collagen VI, with mitochondrial dysfunction related to processes occurring within the inner mitochondrial membrane, such as PTP opening. Such a link can be provided by oxidative stress. In fact, changes in the composition of extracellular matrix might be sensed by plasma membrane integrins that have been shown to convey intracellular signals resulting in increased ROS formation (30). Besides NADPH oxidase activation, mitochondria have been indicated as the main site for integrin-dependent ROS formation (31,32), although the signaling pathways and the mitochondrial sites have not been elucidated yet. Mitochondrial ROS generation, that according to our data is mostly catalyzed by MAO, is likely to be linked to PTP through a vicious cycle whereby an increased ROS formation increases PTP open probability, and vice versa (33). In cardiomyocytes, MAO inhibition was found to reduce ROS formation as well as Tm oxidation, prevent PTP opening and decrease cell death induced by post-ischemic reperfusion (34). In addition, MAO plays a prominent role in cardiomyocyte hypertrophy in vitro and in its progression toward heart failure in vivo (14). These concepts are now extended to skeletal muscle. Indeed the present findings point to mitochondria as the major site, and MAO as the major source, of ROS formation. Previous studies demonstrated the efficacy of N-acetylcysteine or polyphenols from green tea extracts in ameliorating the muscle pathophysiology of *mdx* mice (7,35). However, these drugs can only reduce the level of ROS that are already formed, by acting as a scavenger. Pargyline instead acts by preventing ROS formation, thus making this class of inhibitors much more attractive.

In conclusion, this study provides evidence that MAO-dependent ROS accumulation is a major determinant of both oxidative modifications of myofibrillar proteins and cell death resulting in a marked impairment of contractile function. Therefore, MAO inhibition protects dystrophic skeletal

muscle by reducing ROS production. The possibility of ameliorating the contractile dysfunction in MDs by using MAO inhibitors appears extremely interesting, since these compounds are already used in clinical settings for the treatment of various neurological disorders (12). Therefore these findings provide a solid rationale for exploiting MAO inhibition as a novel therapeutic approach in MDs. In addition, the increased oxidation of Tm in dystrophic muscles (that is reduced upon protective intervention, i.e. MAO inhibition) suggests that oxidative modifications of contractile proteins might be exploited as novel diagnostic tools to evaluate both the severity of the disease and the efficacy of a given treatment.

Materials and Methods

Mice and pargyline treatment *in vivo*. *Col6a1*$^{+/-}$ mice were backcrossed in the inbred C57BL/6J strain for eight generations as described (11), and data were obtained by comparing *Col6a1*$^{-/-}$ mice with their wild-type littermates. Wild-type C57BL/10 mice and *mdx* (in the C57BL/10 background) were obtained from Charles River and Jackson Laboratories, respectively. Pargyline (50 mg/kg/d) or vehicle (phosphate buffered saline, PBS) were administered by daily intraperitoneal injection for 7 d in 6-month-old *Col6a1*$^{-/-}$ and C57BL/6J male mice or 5-week-old *mdx* and C57BL/10 male mice. During the treatment, mice were placed in separate cages with running-wheel. At the end of the treatment, mice were sacrificed and muscles were removed and stored in liquid nitrogen until use. All *in vivo* experiments were approved by the competent Authority of the University of Padova.

MAO activity assay. Muscle cryosections were suspended in PBS and centrifuged at 500g for 10 min at 4°C. The supernatant was centrifuged at 8,000g for 10 min at 4°C and the resulting pellet was resuspended in PBS and stored on ice until use. Protein concentration was determined by the Bradford assay (Bio-Rad). MAO activity assay was based on the detection of hydrogen peroxide generated during substrate catabolism in a horseradish peroxidase (HRP) coupled reaction using 10-acetyl-3,7-dihydroxyphenoxazine (Amplex Red reagent, Molecular Probes). The mitochondrial protein extracts (40 μg) were incubated in PBS with 10 μM Amplex Red and 15 μg/ml HRP. The reaction was started by the addition of 250 μM tyramine, a MAO-A and MAO-B substrate. The fluorescence intensity was recorded at 37°C using a Perkin Elmer LS-50B fluorimeter at the 544/590 nm excitation/emission wavelengths. Parallel samples were run in the absence of substrate to take into account the increase of fluorescence not due to MAO activity.

Dihydroethidium staining for ROS detection. Dihydroethidium (DHE) is oxidized by ROS, forming ethidium bromide, which emits red fluorescence when intercalates with DNA (36). Skeletal muscle

cryosections (10-μm thick) were incubated with 5 μM DHE (Sigma) in PBS at 37°C for 30 min in humid atmosphere and in the dark, washed twice with PBS, mounted and visualized with an Olympus IMT-2 inverted microscope, equipped with a xenon lamp and a 12-bit digital cooled CCD camera (Micromax, Princeton Instruments) as previously described (37). For detection of the fluorescence, 568±25 nm excitation and 585 nm longpass emission filter settings were used. Data were acquired and analysed using Metamorph software (Universal Imaging).

Protein extraction and immunoelectrophoresis. Protein extracts were prepared as described (16). Immunoblotting were stained with the following antibodies: anti-Tm CH1 clone (Sigma), anti-MAO-B D-16 and anti-MAO-A H-70 clone (Santa Cruz). In anti-Tm immunoblots the high molecular mass peptides were attributed to disulfide cross-bridge (DCB) formation by comparing electrophoreses carried out in the absence or in the presence of β-mercaptoethanol as described (16). Quantitation of Tm oxidation was performed by densitometric analysis of the bands obtained under non-reducing conditions (ImageJ software). DCB density was normalized to the actin density in Red Ponceau to take differences in sample loading into account. Data were expressed as percentage of DCB relative to vehicle-treated wild-type mice.

Pathological markers. Cross-sections (7-μm thick) were prepared and processed for haematoxylin and eosin (H&E) staining. For the morphometric analysis of myofiber cross-sectional areas, we counted approximately 2000 fibers per mouse for each muscle type by means of ImageJ software. At least three sections from each muscle were analyzed. TUNEL was performed on paraffin-embedded sections (7-μm thick) using the ApopTag *in situ* apoptosis detection kit (Chemicon). Samples were stained with peroxidase diaminobenzidine to detect TUNEL-positive nuclei and counterstained with Hoechst 33258 to identify all nuclei, as described previously (11). The total number of nuclei and number of TUNEL-positive nuclei were determined in randomly selected fibers using a Zeiss Axioplan microscope

equipped with a Leica DC 500 camera. Membrane permeability of skeletal muscle was directly visualized by immunohistochemical staining with IgG (18,19). Cryosections (10-μm thick) were incubated with anti-mouse fluorescein isothiocyanate-conjugated IgG, washed twice with PBS, mounted and visualized with an Olympus IMT-2 inverted microscope as previously described (37) using excitation/emission cubes of 488/525±25 nm bandpass. Evans blue dye staining of muscles *in vivo* was performed by i.p. injection with 0.2 ml Evans blue (10 mg/ml in phosphate-buffered saline, Sigma). Mice were sacrificed after 16-18 h and diaphragms were fixed with 4% paraformaldehyde overnight at 4°C. After fixation, the samples were observed by means of light microscopy.

Muscle functional assessment. Single myofibers were isolated from *Col6a1*$^{-/-}$ gastrocnemius muscle, chemically skinned as described (38) and tension was measured during maximal isometric activation (pCa = 4.5, T = 20°C, initial sarcomere length = 2.75 μm). Force measurements were performed in the left and/or right gastrocnemius muscle of anaesthetized mice by electrical stimulation through the sciatic nerve, as described previously (19). Voluntary exercise was evaluated by placing a wheel in the cage. Before the treatment, mice were placed in separate cages with wheel to acclimatize, then the average distance covered by each mouse in 24 hours during the treatment was measured using an automatic counter.

Statistics. All data are expressed as the mean ± s.e.m. We analyzed data with the unpaired Student's *t*-test, and values with $P < 0.05$ were considered significant.

Acknowledgements

We thank C. Romualdi for the statistical analysis, C. Mammucari for helpful discussions and A. Pici for performing experiments. This work was supported by grants from the University of Padova (Progetti di Ateneo [CPDA068417] and Fondazione Cariparo); Italian Ministry for University and Research (PRIN); CNR and Telethon Foundation [GGP08107].

Conflict of Interest Statement

The authors declare that they have no financial interests

References

1. Durbeej,M., Campbell,K.P. (2002) Muscular dystrophies involving the dystrophin-glycoprotein complex: an overview of current mouse models. *Curr. Opin. Genet. Dev.*, 12, 349-361.

2. Bonaldo,P., Braghetta,P., Zanetti,M., Piccolo,S., Volpin,D., Bressan,G.M. (1998) Collagen VI deficiency induces early onset myopathy in the mouse: an animal model for Bethlem myopathy. *Human Molecular Genetics*, 7, 2135-2140.

3. Rando,T.A. (2002) Oxidative stress and the pathogenesis of muscular dystrophies. *Am. J. Phys. Med. Rehabil.*, 81, S175-S186.

4. Whitehead,N.P., Yeung,E.W., Allen,D.G. (2006) Muscle damage in mdx (dystrophic) mice: role of calcium and reactive oxygen species. *Clin. Exp. Pharmacol. Physiol*, 33, 657-662.

5. Tidball,J.G., Wehling-Henricks,M. (2007) The role of free radicals in the pathophysiology of muscular dystrophy. *J. Appl. Physiol*, 102, 1677-1686.

6. Messina,S., Bitto,A., Aguennouz,M., Mazzeo,A., Migliorato,A., Polito,F., Irrera,N., Altavilla,D., Vita,G.L., Russo,M., *et al.* (2009) Flavocoxid counteracts muscle necrosis and improves functional properties in mdx mice: a comparison study with methylprednisolone. *Exp. Neurol.*, 220, 349-358.

7. Whitehead,N.P., Pham,C., Gervasio,O.L., Allen,D.G. (2008) N-Acetylcysteine ameliorates skeletal muscle pathophysiology in mdx mice. *J. Physiol*, 586, 2003-2014.

8. Disatnik,M.H., Dhawan,J., Yu,Y., Beal,M.F., Whirl,M.M., Franco,A.A., Rando,T.A. (1998) Evidence of oxidative stress in mdx mouse muscle: studies of the pre-necrotic state. *J. Neurol. Sci.*, 161, 77-84.

9. Millay,D.P., Sargent,M.A., Osinska,H., Baines,C.P., Barton,E.R., Vuagniaux,G., Sweeney,H.L., Robbins,J., Molkentin,J.D. (2008) Genetic and pharmacologic inhibition of mitochondrial-dependent necrosis attenuates muscular dystrophy. *Nat. Med.*, 14, 442-447.

10. Palma,E., Tiepolo,T., Angelin,A., Sabatelli,P., Maraldi,N.M., Basso,E., Forte,M.A., Bernardi,P., Bonaldo,P. (2009) Genetic ablation of cyclophilin D rescues mitochondrial defects and prevents muscle apoptosis in collagen VI myopathic mice. *Hum. Mol. Genet.*, 18, 2024-2031.

11. Irwin,W.A., Bergamin,N., Sabatelli,P., Reggiani,C., Megighian,A., Merlini,L., Braghetta,P., Columbaro,M., Volpin,D., Bressan,G.M., *et al.* (2003) Mitochondrial dysfunction and apoptosis in myopathic mice with collagen VI deficiency. *Nature Genetics*, 35, 367-371.

12. Youdim,M.B., Edmondson,D., Tipton,K.F. (2006) The therapeutic potential of monoamine oxidase inhibitors. *Nat. Rev. Neurosci.*, 7, 295-309.

13. Bianchi,P., Kunduzova,O., Masini,E., Cambon,C., Bani,D., Raimondi,L., Seguelas,M.H., Nistri,S., Colucci,W., Leducq,N., Parini,A. (2005) Oxidative stress by monoamine oxidase mediates receptor-independent cardiomyocyte apoptosis by serotonin and postischemic myocardial injury. *Circulation*, 112, 3297-3305.

14. Kaludercic,N., Takimoto,E., Nagayama,T., Feng,N., Lai,E.W., Bedja,D., Chen,K., Gabrielson,K.L., Blakely,R.D., Shih,J.C., *et al.* (2010) Monoamine oxidase A-mediated

enhanced catabolism of norepinephrine contributes to adverse remodeling and pump failure in hearts with pressure overload. *Circ. Res.*, 106, 193-202.

15. Canton,M., Neverova,I., Menabò,R., Van Eyk,J.E., Di Lisa,F. (2004) Evidence of myofibrillar protein oxidation induced by postischemic reperfusion in isolated rat hearts. *Am. J. Physiol Heart Circ. Physiol*, 286, H870-H877.

16. Canton,M., Skyschally,A., Menabo,R., Boengler,K., Gres,P., Schulz,R., Haude,M., Erbel,R., Di Lisa,F., Heusch,G. (2006) Oxidative modification of tropomyosin and myocardial dysfunction following coronary microembolization. *Eur. Heart J.*, 27, 875-881.

17. Sicinski,P., Geng,Y., Ryder-Cook,A.S., Barnard,E.A., Darlison,M.G., Barnard,P.J. (1989) The molecular basis of muscular dystrophy in the mdx mouse: a point mutation. *Science*, 244, 1578-1580.

18. Weller,B., Karpati,G., Carpenter,S. (1990) Dystrophin-deficient mdx muscle fibers are preferentially vulnerable to necrosis induced by experimental lengthening contractions. *J. Neurol. Sci.*, 100, 9-13.

19. Blaauw,B., Mammucari,C., Toniolo,L., Agatea,L., Abraham,R., Sandri,M., Reggiani,C., Schiaffino,S. (2008) Akt activation prevents the force drop induced by eccentric contractions in dystrophin-deficient skeletal muscle. *Hum. Mol. Genet.*, 17, 3686-3696.

20. Blaauw,B., Agatea,L., Toniolo,L., Canato,M., Quarta,M., Dyar,K.A., Danieli-Betto,D., Betto,R., Schiaffino,S., Reggiani,C. (2010) Eccentric contractions lead to myofibrillar dysfunction in muscular dystrophy. *J. Appl. Physiol*, 108, 105-111.

21. Sampaolesi,M., Torrente,Y., Innocenzi,A., Tonlorenzi,R., D'Antona,G., Pellegrino,M.A., Barresi,R., Bresolin,N., De Angelis,M.G., Campbell,K.P., *et al.* (2003) Cell therapy of alpha-sarcoglycan null dystrophic mice through intra-arterial delivery of mesoangioblasts. *Science*, 301, 487-492.

22. Disatnik,M.H., Chamberlain,J.S., Rando,T.A. (2000) Dystrophin mutations predict cellular susceptibility to oxidative stress. *Muscle Nerve*, 23, 784-792.

23. Merlini,L., Angelin,A., Tiepolo,T., Braghetta,P., Sabatelli,P., Zamparelli,A., Ferlini,A., Maraldi,N.M., Bonaldo,P., Bernardi,P. (2008) Cyclosporin A corrects mitochondrial dysfunction and muscle apoptosis in patients with collagen VI myopathies. *Proc. Natl. Acad. Sci. U. S. A*, 105, 5225-5229.

24. Berlett,B.S., Stadtman,E.R. (1997) Protein oxidation in aging, disease, and oxidative stress. *J. Biol. Chem.*, 272, 20313-20316.

25. Michele,D.E., Metzger,J.M. (2000) Physiological consequences of tropomyosin mutations associated with cardiac and skeletal myopathies. *J. Mol. Med.*, 78, 543-553.

26. Bottinelli,R., Coviello,D.A., Redwood,C.S., Pellegrino,M.A., Maron,B.J., Spirito,P., Watkins,H., Reggiani,C. (1998) A mutant tropomyosin that causes hypertrophic cardiomyopathy is expressed in vivo and associated with an increased calcium sensitivity. *Circ. Res.*, 82, 106-115.

27. Angelin,A., Tiepolo,T., Sabatelli,P., Grumati,P., Bergamin,N., Golfieri,C., Mattioli,E., Gualandi,F., Ferlini,A., Merlini,L., *et al.* (2007) Mitochondrial dysfunction in the pathogenesis

of Ullrich congenital muscular dystrophy and prospective therapy with cyclosporins. *Proc. Natl. Acad. Sci. U. S. A*, 104, 991-996.

28. Tiepolo,T., Angelin,A., Palma,E., Sabatelli,P., Merlini,L., Nicolosi,L., Finetti,F., Braghetta,P., Vuagniaux,G., Dumont,J.M., *et al.* (2009) The cyclophilin inhibitor Debio 025 normalizes mitochondrial function, muscle apoptosis and ultrastructural defects in Col6a1(-/-) myopathic mice. *Br. J. Pharmacol.*, 157, 1045-1052.

29. Reutenauer,J., Dorchies,O.M., Patthey-Vuadens,O., Vuagniaux,G., Ruegg,U.T. (2008) Investigation of Debio 025, a cyclophilin inhibitor, in the dystrophic mdx mouse, a model for Duchenne muscular dystrophy. *Br. J. Pharmacol.*, 155, 574-584.

30. Svineng,G., Ravuri,C., Rikardsen,O., Huseby,N.E., Winberg,J.O. (2008) The role of reactive oxygen species in integrin and matrix metalloproteinase expression and function. *Connect. Tissue Res.*, 49, 197-202.

31. Werner,E., Werb,Z. (2002) Integrins engage mitochondrial function for signal transduction by a mechanism dependent on Rho GTPases. *J. Cell Biol.*, 158, 357-368.

32. Taddei,M.L., Parri,M., Mello,T., Catalano,A., Levine,A.D., Raugei,G., Ramponi,G., Chiarugi,P. (2007) Integrin-mediated cell adhesion and spreading engage different sources of reactive oxygen species. *Antioxid. Redox. Signal.*, 9, 469-481.

33. Di Lisa,F., Bernardi,P. (2009) A CaPful of mechanisms regulating the mitochondrial permeability transition. *J. Mol. Cell Cardiol.*, 46, 775-780.

34. Di,L.F., Kaludercic,N., Carpi,A., Menabo,R., Giorgio,M. (2009) Mitochondrial pathways for ROS formation and myocardial injury: the relevance of p66(Shc) and monoamine oxidase. *Basic Res. Cardiol.*, 104, 131-139.

35. Dorchies,O.M., Wagner,S., Vuadens,O., Waldhauser,K., Buetler,T.M., Kucera,P., Ruegg,U.T. (2006) Green tea extract and its major polyphenol (-)-epigallocatechin gallate improve muscle function in a mouse model for Duchenne muscular dystrophy. *Am. J. Physiol Cell Physiol*, 290, C616-C625.

36. Benov,L., Sztejnberg,L., Fridovich,I. (1998) Critical evaluation of the use of hydroethidine as a measure of superoxide anion radical. *Free Radic. Biol. Med.*, 25, 826-831.

37. Petronilli,V., Miotto,G., Canton,M., Brini,M., Colonna,R., Bernardi,P., Di Lisa,F. (1999) Transient and long-lasting openings of the mitochondrial permeability transition pore can be monitored directly in intact cells by changes in mitochondrial calcein fluorescence. *Biophys. J.*, 76, 725-734.

38. Rossi,R., Bottinelli,R., Sorrentino,V., Reggiani,C. (2001) Response to caffeine and ryanodine receptor isoforms in mouse skeletal muscles. *Am. J. Physiol Cell Physiol*, 281, C585-C594.

Figure Legends

Figure 1. MAO inhibition reduces oxidative stress in *Col6a1*$^{-/-}$ mice. (**A**) MAO activity in gastrocnemius muscles from wild-type and *Col6a1*$^{-/-}$ mice after one week of treatment with pargyline or vehicle. (**B**) Representative western blots (WB) of MAO-A and MAO-B in diaphragm and gastrocnemius from wild-type (n = 6) and *Col6a1*$^{-/-}$ (n = 6) mice. Equal protein loading was indicated by red Ponceau staining. (**C**) Oxidative stress, assessed by dihydroethidium (DHE) staining in sections of diaphragm from vehicle- or pargyline-treated wild-type and *Col6a1*$^{-/-}$ mice. Scale bar, 50 μm. (**D**) Quantification of DHE fluorescence in gastrocnemius, diaphragm and tibialis anterior (TA) muscle cryosections from wild-type and *Col6a1*$^{-/-}$ mice treated with vehicle or pargyline showing the reduced ROS accumulation after pargyline treatment. Parg, pargyline; veh, vehicle; WT, wild-type. * P<0.05 *Col6a1*$^{-/-}$-veh versus WT-veh; # P<0.05 *Col6a1*$^{-/-}$-veh versus *Col6a1*$^{-/-}$-parg. Error bars represent s.e.m. The number of mice for each group is indicated inside each bar.

Figure 2. MAO inhibition reduces Tm oxidation in *Col6a1*$^{-/-}$ mice. (**A**) Tm oxidation detected as formation of disulfide cross-bridge (DCB) in diaphragm muscles of vehicle- or pargyline-treated wild-type and *Col6a1*$^{-/-}$ mice. High molecular mass peptides were attributed to DCB formation by comparing electrophoreses carried out in the absence or in the presence of β-mercaptoethanol (β-me). Immunoblotting displayed additional high molecular mass bands in *Col6a1*$^{-/-}$ diaphragm that were reduced by pargyline treatment. (**B**) Quantitative analysis of DCB formation in Tm immunoblots showing a significant decrease of Tm oxidation upon pargyline treatment . Parg, pargyline; veh, vehicle; WT, wild-type. * P<0.05 *Col6a1*$^{-/-}$-veh versus WT-veh; # P<0.05 *Col6a1*$^{-/-}$-veh versus *Col6a1*$^{-/-}$-parg. Error bars represent s.e.m. The number of mice for each group is indicated inside each bar.

Figure 3. MAO inhibition rescues histological alterations and prevents muscle apoptosis in *Col6a1*$^{-/-}$ mice. (**A**) Quantification of apoptotic nuclei by TUNEL assay in diaphragm sections. Pargyline treatment prevented the increased incidence of apoptosis in *Col6a1*$^{-/-}$ mice. (**B**) Quantification of the necrotic fibers by means of the immunohistochemical staining for IgG in diaphragm sections. IgG-positive fibers were present in *Col6a1*$^{-/-}$ mice and their number was decreased by pargyline treatment. (**C**) Representative images of diaphragms from wild-type and *Col6a1*$^{-/-}$ mice, following vital staining with Evans blue dye. Diaphragms were isolated from wild-type (n=5) and *Col6a1*$^{-/-}$ (n=5) mice treated with vehicle or pargyline, and examined by light microscopy. Diaphragms from *Col6a1*$^{-/-}$ mice displayed a marked incidence of damaged fibers, identified by deep blue striations, which was reduced after pargyline treatment. (**D**) Representative cross-sections of H&E-staining from tibialis anterior muscle from wild-type and *Col6a1*$^{-/-}$ mice treated with vehicle or pargyline. *Col6a1*$^{-/-}$ muscles showed a large variability in myofiber size while pargyline-treated *Col6a1*$^{-/-}$ mice displayed uniform myofiber size, similarly to wild-type muscles. Scale bar, 100 μm. (**E**) Analysis of fiber cross-sectional areas (CSA) in diaphragm and tibialis anterior (TA) muscle of pargyline- or vehicle-treated wild-type and *Col6a1*$^{-/-}$ mice. Parg, pargyline; veh, vehicle; WT, wild-type. * P<0.05 *Col6a1*$^{-/-}$-veh versus WT-veh; # P<0.05 *Col6a1*$^{-/-}$-veh versus *Col6a1*$^{-/-}$-parg. Error bars represent s.e.m. The number of mice for each group is indicated inside each bar. The key in **A** applies to all panels.

Figure 4. MAO inhibition ameliorates muscle alterations in *Col6a1*$^{-/-}$ mice. (**A**) Tension development by single skinned fibers of gastrocnemius from vehicle-treated *Col6a1*$^{-/-}$, pargyline-treated *Col6a1*$^{-/-}$ and vehicle-treated wild-type mice. *Col6a1*$^{-/-}$ muscles developed lower isometric tension than wild-type fibers. The contractile impairment disappeared in the fibers of pargyline-treated *Col6a1*$^{-/-}$ mice. n = 22 or more fibers for each group. (**B**) Force-frequency curves of gastrocnemius muscle from vehicle-treated or pargyline-treated *Col6a1*$^{-/-}$ mice showed a significant increase of the normalized force of gastrocnemius muscle upon pargyline treatment. n = 13 or more muscles for each

group. P=0.0016 by a two-way analysis of variance. (**C**) Locomotor performance measured on the running-wheel as the average distance covered in 24 h. Pargyline-treated *Col6a1*$^{-/-}$ mice showed a significant recovery of the exercise performance. Parg, pargyline; veh, vehicle; WT, wild-type. * P<0.05 *Col6a1*$^{-/-}$-veh versus WT-veh; # P<0.05 *Col6a1*$^{-/-}$-veh versus *Col6a1*$^{-/-}$-parg. Error bars represent s.e.m. The number of mice for each group is indicated inside each bar or between parentheses for panel **B**. The key in **A** applies to all panels.

Figure 5. Pargyline treatment reduces Tm oxidation in *mdx* mice. (**A**) DCB formation in Tm detected by immunoelectrophoresis of myofibrillar samples from gastrocnemius and quadriceps muscles, as detailed in Figure 2A. Immunoblotting analyses showed that the additional high molecular mass bands in *Col6a1*$^{-/-}$ muscles were significantly reduced by pargyline treatment (**B**) Quantitative analysis of DCB formation in Tm immunoblots. Parg, pargyline; veh, vehicle; WT, wild-type, β-mercaptoethanol (β-me). * P<0.05 *mdx*-veh versus WT-veh; # P<0.05 *mdx*-veh versus *mdx*-parg. Error bars represent s.e.m. The number of mice for each group is indicated inside each bar.

Figure 6. Pargyline treatment ameliorates dystrophic pathology in *mdx* mice.
(**A**) Representative cross-sections of H&E-staining of gastrocnemius (Gastroc.) and quadriceps (Quadr.) muscles from wild-type and *mdx* mice treated with vehicle or with pargyline. *Mdx* muscles showed a large variability in myofiber size and occurrence of inflammatory infiltrates (arrows). On the contrary, *mdx* treated mice displayed uniform fibers size and absence of inflammatory infiltrates, similarly to wild-type muscles. Scale bar, 100 μm. (**B**) Morphometric analysis of myofiber cross-sectional areas (CSA) in gastrocnemius muscles of wild-type and *mdx* mice treated with vehicle or pargyline. (**C**) Quantification of apoptotic nuclei by TUNEL assay in diaphragm muscle sections. Pargyline treatment blunted the increased incidence of apoptosis in *mdx* mice. Parg, pargyline; veh, vehicle; WT, wild-type, β-mercaptoethanol (β-me). * P<0.05 *mdx*-veh versus WT-veh; # P<0.05 *mdx*-

veh versus *mdx*-parg. Error bars represent s.e.m. The number of mice for each group is indicated inside each bar.

Table 1. Pargyline treatment reduces MAO-dependent ROS formation in *mdx* mice.

DHE Staining (% relative to WT-veh)

	Gastrocnemius	Quadriceps
WT-veh mice (n=8)	100.0 ± 8.4	100.0 ± 8.3
mdx-veh mice (n=8)	127.8 ± 9.0 *	119.3 ± 1.3*
WT-parg mice (n=8)	102.8 ± 2.8	96.9 ± 6.2
mdx-parg mice (n=8)	105.6 ± 2.2 #	102.9 ± 1.5 #

Accumulation of ROS, quantified by increased DHE fluorescence, in gastrocnemius and quadriceps muscle from wild-type and *mdx* mice treated with vehicle or pargyline. Parg, pargyline; veh, vehicle; WT, wild-type. * $P<0.05$ *mdx*-veh versus WT-veh; # $P<0.05$ *mdx*-veh versus *mdx*-parg. Data represent means ± s.e.m. The number of mice for each group is indicated between parentheses.

Abbreviations

ROS = reactive oxygen species

MD = muscular dystrophy

MAO = monoamine oxidase

Tm = tropomyosin

DHE = dihydroethidium

DCB = disulphide cross-bridge

TUNEL = terminal deoxynuleotidyl transferase-mediates dUTP nick and labeling

TA = tibialis anterior

β-me = β-mercaptoethanol

H&E-staining = haematoxylin and eosin staining

CSA = cross-sectional area

PBS = phosphate buffered saline

Figure 1.

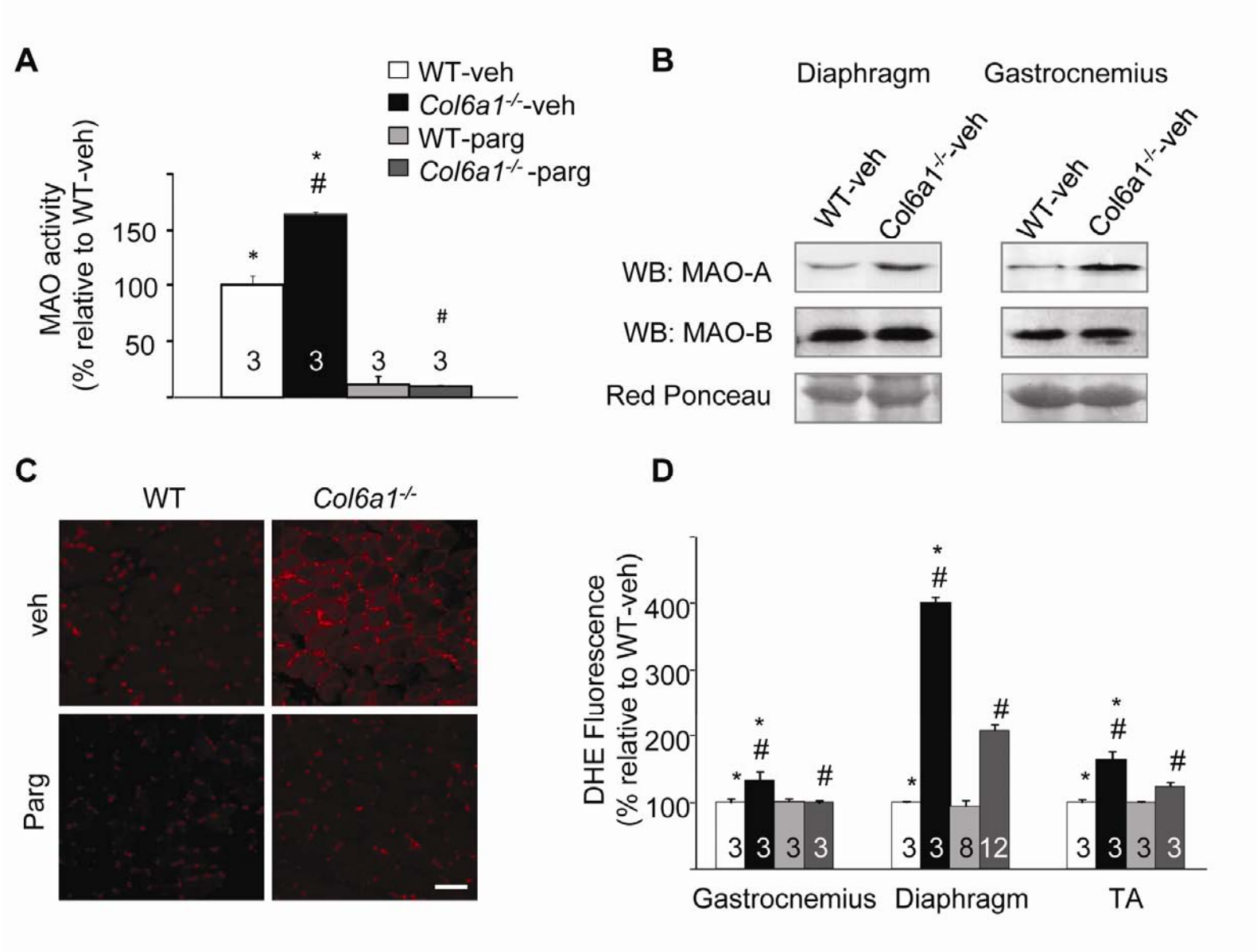

Figure 2.

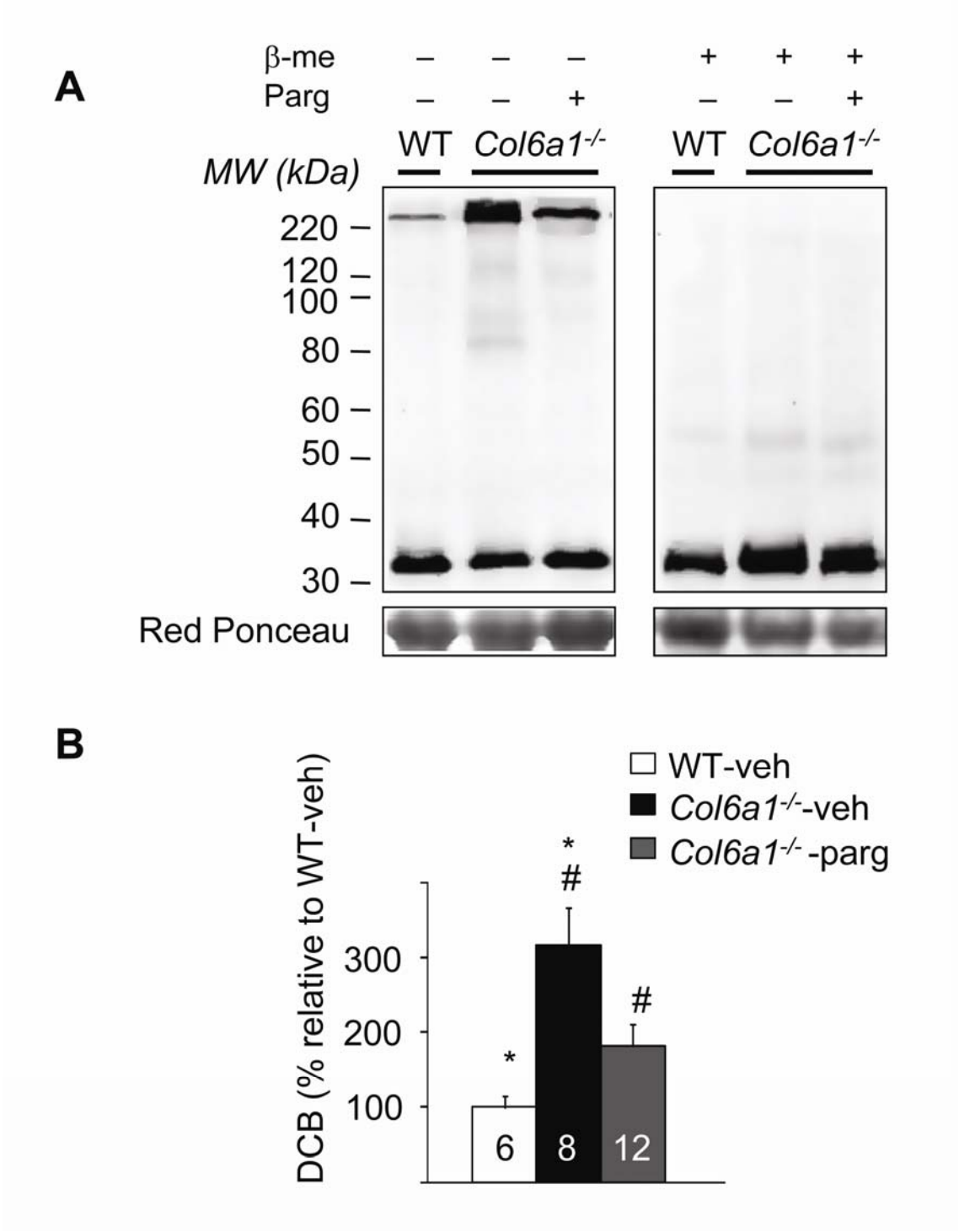

Figure 3.

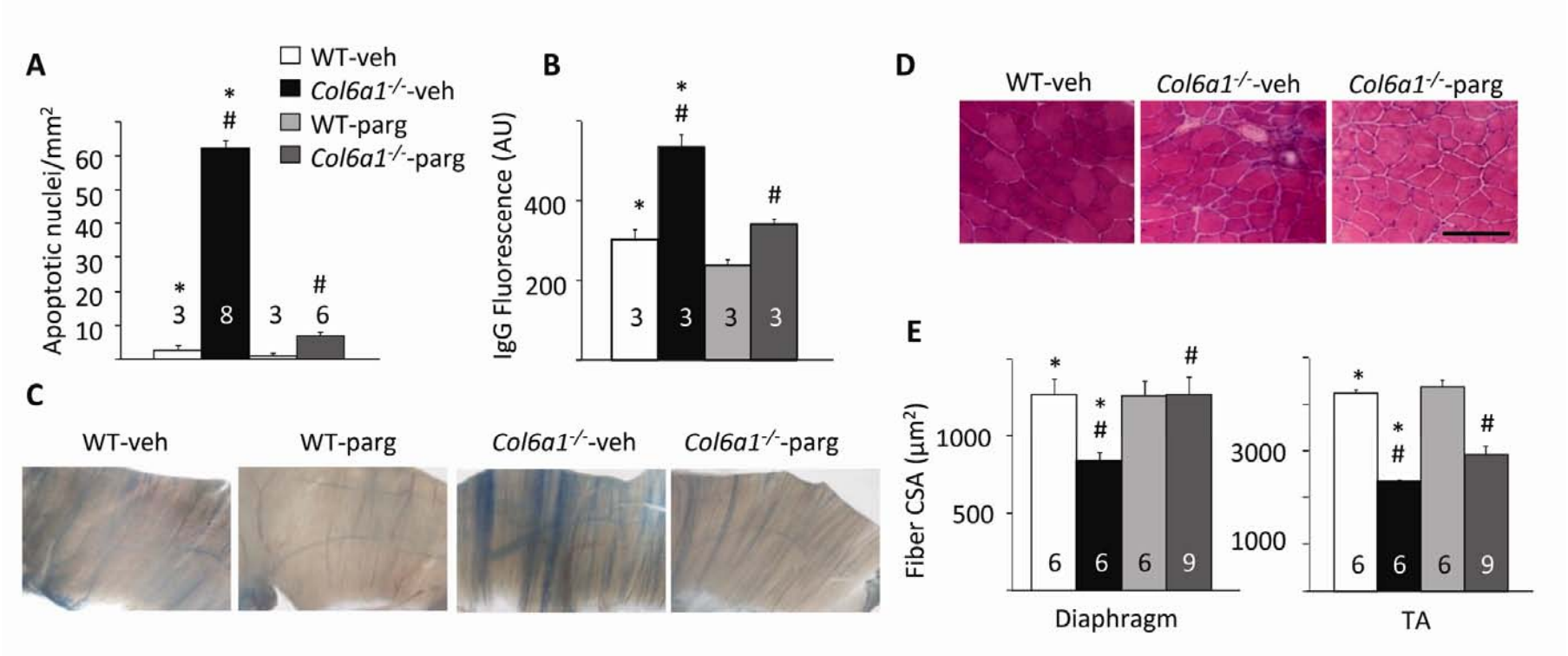

Figure 4.

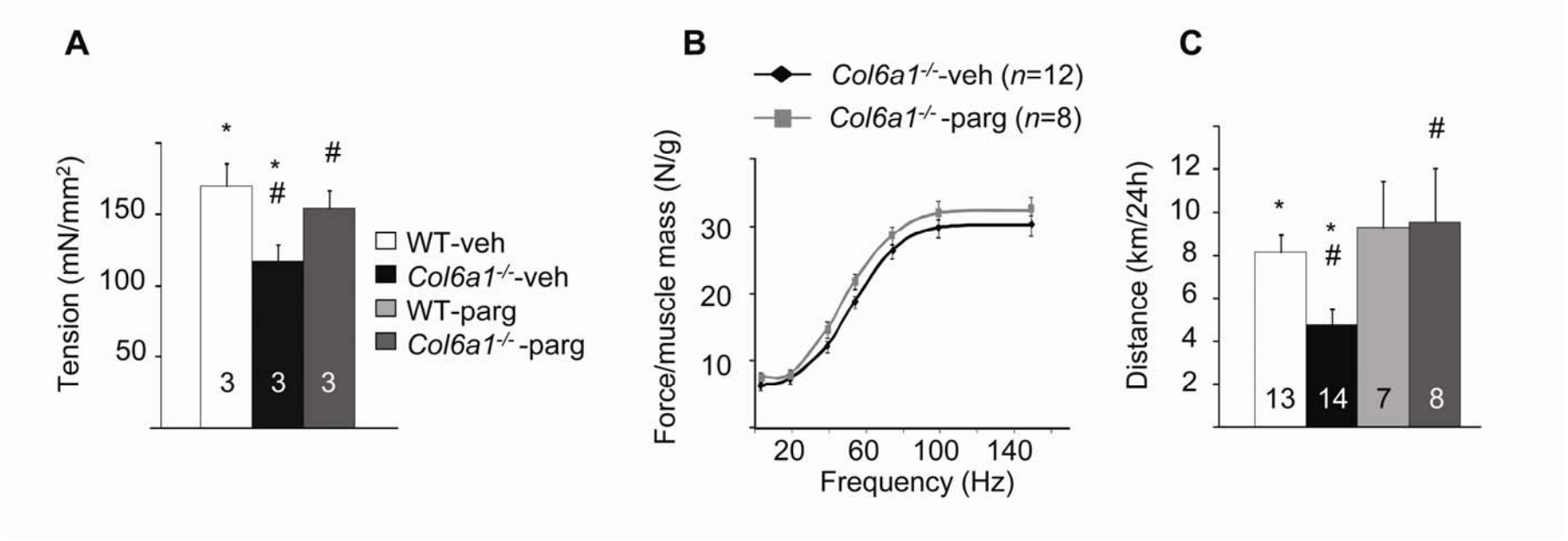

Figure 5.

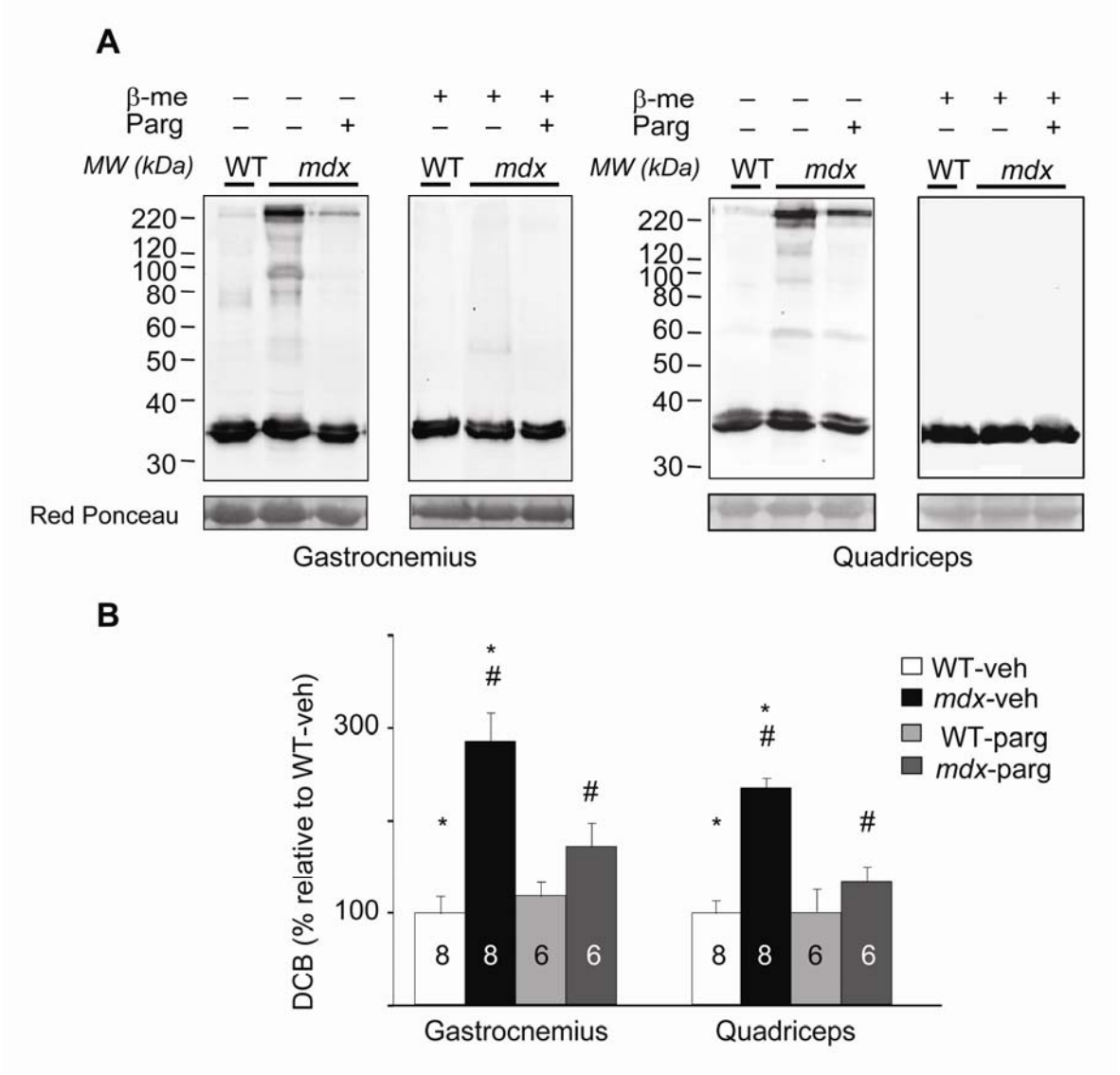

Figure 6.